International Journal of Heat and Mass Transfer 52 (2009) 767–776

Contents lists available at ScienceDirect

International Journal of Heat and Mass Transfer

journal homepage: www.elsevier.com/locate/ijhmt

Bubble growth with chemical reactions in microchannels

B.R. Fu, Chin Pan *

Department of Engineering and System Science, National Tsing Hua University, 101, Section 2, Kuang-Fu Road, Hsinchu 30043, Taiwan, ROC

ARTICLE INFO

Article history:
Received 6 December 2007
Received in revised form 2 July 2008
Available online 11 September 2008

Keywords:
Bubble growth
Microchannel
Two-phase flow
Chemical reaction

ABSTRACT

This work investigates the nucleation and growth of CO_2 bubbles due to chemical reactions of sulfuric acid and sodium bicarbonate in three types of microchannels: one with uniform cross-section, one converging, and another one diverging. The Y-shaped test section, composed of main and two front microchannels, was made of P-type ⟨100⟩ orientation SOI (silicon on insulator) wafer. Bubble nucleation and growth in microchannels under various conditions were observed using a high-speed digital camera. The theoretical model for bubble dynamics with a chemical reaction is reviewed or developed. In the present study, no bubble was nucleated at the given inlet concentration and in the range of flow rate in the converging microchannel while the nucleation and growth of bubbles were observed in the diverging and uniform cross-section microchannels. Bubbles are nucleated at the channel wall and the equivalent bubble radius increases linearly during the initial period of the bubble growth. The bubble growth behavior for a particular case, without relative motion between the bubble and liquid, shows that the mass diffusion controls the bubble growth; consequently, the bubble radius grows as a square root of the time and agrees very well with the model in the literature. On the other hand, for other cases the bubbles stay almost at the nucleation site while growing with a constant gas product generation rate resulting in the instant bubble radius following the one-third power of the time.

1. Introduction

Bubble generation, growth, and interactions in a microchannel due to chemical reactions are of significant interest for the design of the microchannel reactor involving gas–liquid reactions or devices concerning the generation of bubbles due to chemical reactions. For example, CO_2 bubbles are generated from the oxidation of methanol in the anode of a direct methanol fuel cell (DMFC). CO_2 may then transport through the diffusion layer to the fuel channel. The removal of CO_2 bubbles is of critical concern for the design of a micro-DMFC [1–6].

Bubble dynamics for convective boiling in single and two parallel microchannels had been investigated by Lee et al. [7] and Li et al. [8], respectively. Both studies reported that bubbles in microchannels typically grow linearly and the bubble departure is governed by the imbalance of two-phase flow drag over the surface tension. The two-phase flow pattern rapidly evolves to slug flow after the bubble departure. The length of bubble slug expands exponentially in both forward and backward directions, resulting from the evaporation of microlayer between the bubble slug and heating wall. Recently, Li and Dhir [9] carried out the single bubble dynamics during nucleate flow boiling experimentally and numerically. They found that the bulk flow velocity, heater surface orientation, and gravity levels influence the bubble dynamics.

Bubble nucleation and growth from the superheated or supersaturated liquid have been extensively studied in the literature, and a number of mathematical models for bubble growth are available [10–21]. For example, Lee et al. [19] explored experimentally a single bubble growth in saturated nucleate pool boiling with a constant wall temperature. They reported that the bubble radius grows as the 1/5 power of the time. Lee et al. [20] investigated the bubble growth of binary mixtures in saturated pool boiling and found that the bubble radius is proportional to the 1/4–1/6 power of the time. Recently, Frank et al. [21] demonstrated the bubble nucleation and growth in supersaturated liquid with a CO_2 gas under different pressures experimentally. They found that the bubble radius increases linearly before the bubble departure. After the bubble detaches from the nucleation site to rise in the liquid, it grows exponentially.

Nevertheless, there are very few experimental studies related to the bubble growth with chemical reactions in the literature. The nucleation of bubbles produced from chemical reactions is fundamentally different from that of boiling. A bubble is nucleated in a boiling system due to aggregate of high energy, vapor-like molecules and subsequently grows owing to liquid evaporation. Its growth is limited by the liquid inertia or heat conduction in the liquid to transport heat from superheated liquid to the bubble surface to provide the latent heat of evaporation. On the other

* Corresponding author. Tel.: +886 35725363; fax: +886 35720724.
E-mail address: cpan@ess.nthu.edu.tw (C. Pan).

0017-9310/$ - see front matter © 2008 Elsevier Ltd. All rights reserved.
doi:10.1016/j.ijheatmasstransfer.2008.07.018

Nomenclature

a	dimensionless number
b_0	dimensionless number
C_i	constant in the corresponding equation, $i = 1,2,3,4$
c	molar concentration of the solute in the liquid (mol/m^3)
c_s	molar concentration of the solute at the bubble surface (mol/m^3)
c_∞	molar concentration of the solute far from the bubble (mol/m^3)
D	diffusion coefficient (m^2/s)
D_b	bubble diameter of the top-view image (m)
D_H	hydraulic diameter of the microchannel (m)
H	depth of the microchannel (m)
k_m	average mass-transfer coefficient (m/s)
k_s	first-order surface reaction constant (m/s)
n	number of moles of the product within the bubble (mol)
n_g	generation rate of the gas product (mol/s)
P_b	pressure in the bubble (Pa)
P_{b0}	initial pressure in the bubble (Pa)
P_l	pressure in the liquid (Pa)
Q	volume flow rate of the solution (m^3/s)
R_0	initial bubble radius (m)
R_b	instant bubble radius or equivalent bubble radius (m)
$R_{b,cr}$	critical bubble radius (m)
R_g	universal gas constant (J/mol K)
Re_b	Reynolds number based on the bubble diameter and relative velocity between the bubble and liquid
r	radial coordinate
Sc	Schmidt number
Sh	Sherwood number
T_b	temperature in the bubble (K)
t	time (s)
u_r	relative velocity between the sphere and bulk liquid (m/s)

Greek symbols

β	dimensionless growth constant in Eq. (6)
μ_l	viscosity of the liquid (N s/m^2)
ρ_l	density of the liquid (kg/m^3)
σ	surface tension (N/m)
τ_0	dimensionless time

hand, bubble growth due to chemical reactions results from the gas produced at or near the bubble surface. The solute for chemical reactions at the bubble surface or gas generated nearby will diffuse to the bubble surface through concentration gradient. Therefore, bubble growth due to chemical reactions may be similar to boiling bubbles as the governing laws for heat and mass transfer are similar to each other. Kapilashrami et al. [22] employed the CCD cameras to observe the bubble generated through chemical reactions between two immiscible liquids in the transparent box. They found that the bubbles increase in size with progress of reaction but the change in bubble size seems to be independent of the reaction rate. Hong and Woo [23] employed the fractional derivatives method to study bubble growth/dissolution processes with a first-order chemical reaction. Recently, Favelukis and Yablonsky [24] presented a theoretical model for the growth of a spherical bubble in a quiescent liquid with a first-order chemical reaction at the bubble surface.

Recently, Fu et al. [25] investigated experimentally the evolution of two-phase flow pattern with CO_2 bubbles generated from chemical reactions of sulfuric acid and sodium bicarbonate in converging and diverging microchannels with a common inlet chamber, which may cause the pre-mixing effect, especially for the diverging microchannel with a narrow inlet. Much more intensive chemical reactions in the diverging microchannel were demonstrated. CO_2 bubbles are found to be generated in the regions near the exit even for low concentration and high flow rates in the diverging microchannel of their study. Extensive bubble generation and many bubbles are produced in those regions at high concentrations and/or low flow rates. In particular, slug flow with large bubble slugs tends to appear in most parts of the diverging microchannel for low concentrations. On the contrary, no bubble is formed for low concentrations and high flow rates in the converging microchannel, while large spherical bubbles are generated in the regions near the inlet and slug flow is formed in the regions near the exit for high inlet concentrations and low flow rates.

The objectives of the present work are to study experimentally and theoretically the bubble dynamics in microchannels with CO_2 bubbles generated from chemical reactions of sulfuric acid (H_2SO_4) and sodium bicarbonate ($NaHCO_3$). The reaction is, in fact, the following: $H^+ + HCO_3^- \rightarrow CO_2 + H_2O$, which can be regarded as a first-order chemical reaction with a rate constant of $18 \pm 7\ s^{-1}$ [26]. The reactions will take place in the microchannel while the reactant solutions are flowing through it and result in generation of CO_2 in the microchannel. Bubble growth in three different types of microchannels, namely, converging, diverging, and uniform cross-section microchannel are observed and measured. The theoretical model in the literature has been reviewed and a new model is developed based on the experimental data.

2. Experimental detail

2.1. Experimental setup

The experimental setup is similar to that employed in the previous work [25,27]. As shown in Fig. 1, it consists of the test section, a syringe pump (KD Scientific 200), a pressure transducer (Huba 692), a flow visualization system, and a data acquisition system (YOKOGAWA MX100). The syringe pump with two tubes drove the two solutions to different inlet chambers of the test section simultaneously, as shown in the test section layout in Fig. 1. The two liquid streams meet at the intersection of the two front and main channels. The exhausted fluids from the test section were drained to a container on an electronic balance, which provided calibration of the flow rate for each solution before an experiment. The pressure taps were located near the inlet and outlet chambers at the connecting glass tube. The differential pressure transducer used in the present study is with a short response time of 0.005 s and the sampling rate for pressure drop measurement was set at 100 Hz.

The flow visualization system included a high-speed digital camera (KODAK motion coder SR-ultra) with a monitor and a personal computer. A micro-lens was mounted on the CCD to observe the nucleation and growth of bubbles in microchannels. Moreover, an x–y–z mechanism was installed with the test module to hold the lens and provide accurate position on the test plane (x–y-plane) and focusing (z-direction). Bubble nucleation and growth in microchannels under various conditions were observed using the high-speed digital camera and analyzed by the Image Pro.

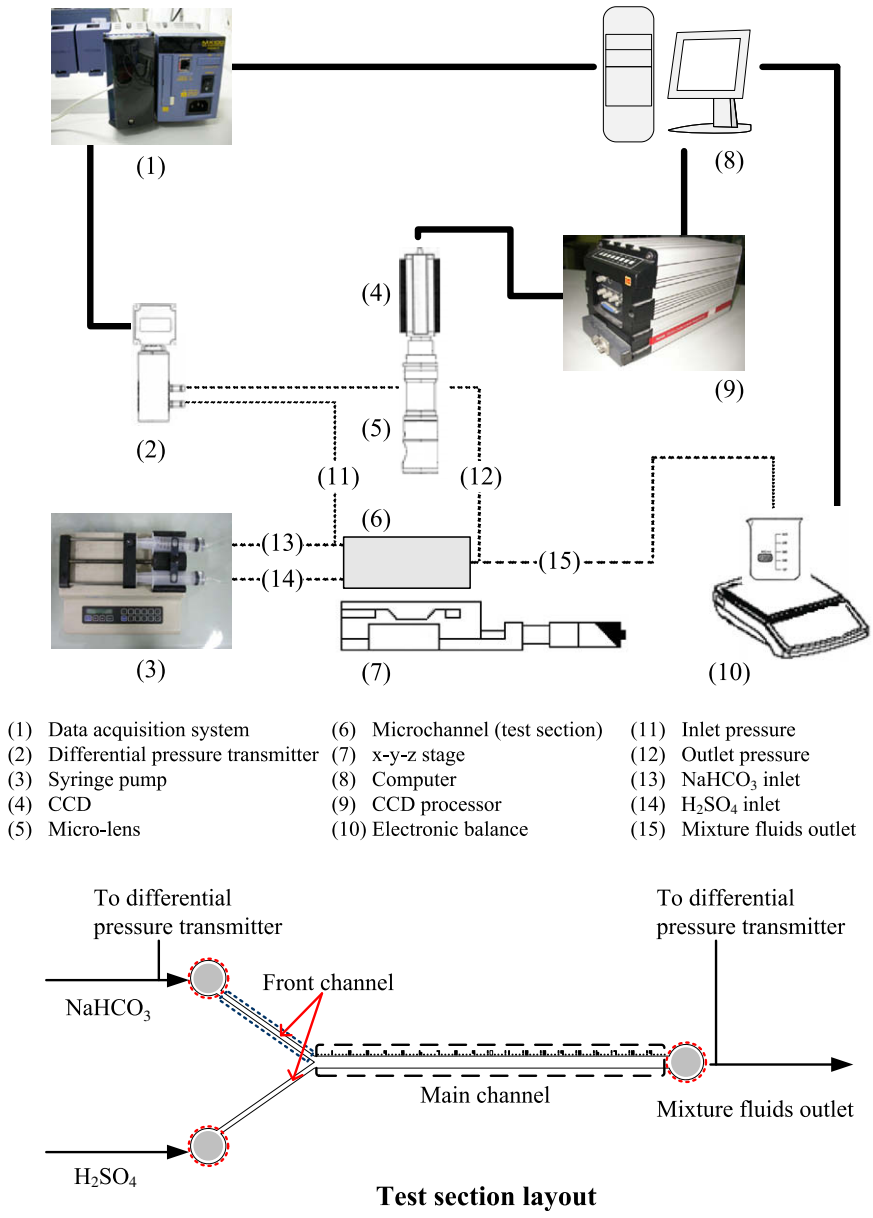

Fig. 1. Schematic of experimental apparatus and the test section layout.

The typical frame rate used was 2000 frame/s and the exposure time was 1/20,000 s. A 250 W fiber optic illuminator was used as the light source.

2.2. Fabrication of the test section

In this study, unlike the design in the previous work [25], the test section was designed without the common inlet mixing chamber, which may cause the pre-mixing effect, especially for the diverging microchannel with a narrow inlet. Consequently, the bubble nucleation and growth will be a result of the situation in the microchannel only. The Y-shaped test section, composed of main and two front microchannels, was a 17.5 mm × 35 mm silicon stripe, which was made of P-type ⟨100⟩ orientation SOI (silicon on insulator) wafer with double sides polished (SWIFTEK Corp.). The SOI wafer, used in this study, consists of three basic layers, from bottom to top: the handle layer (P-type ⟨100⟩ silicon wafer with a thickness of 500 ± 10 μm), the box layer (SO_2 with a thickness of 0.2 μm), and the device layer (P-type ⟨100⟩ silicon with a thickness of 100 ± 1 μm), respectively. The fabrication of the microchannel employed bulk micromachining and anodic bonding process. Using the etching stop mechanism at the box layer for the deep reactive ion etching process, a uniform depth of microchannel can be obtained. Subsequently, the direct writing of excimer laser micromachining technology was applied for the through holes of both fluid inlets and outlet. To enable flow visualization, the top surface was covered with Pyrex #7740 glass through anodic bonding.

The schematic of the Y-shaped test section are shown in Fig. 2(a)–(c) for the main channel with uniform, converging, and diverging cross-section, respectively. The width of the uniform cross-section microchannel is 675 μm, while it varies linearly from 1500 to 210 μm for the converging microchannel and from 210 to 1500 μm for the diverging one resulting in a converging or diverging angle of 1.85°. The length and depth of the main channel, no matter what type the channel is, are 20 mm and 100 μm, respectively. The mean hydraulic diameter (D_H) of the three kinds of main channel is all approximately 174 μm. Both front channels are with

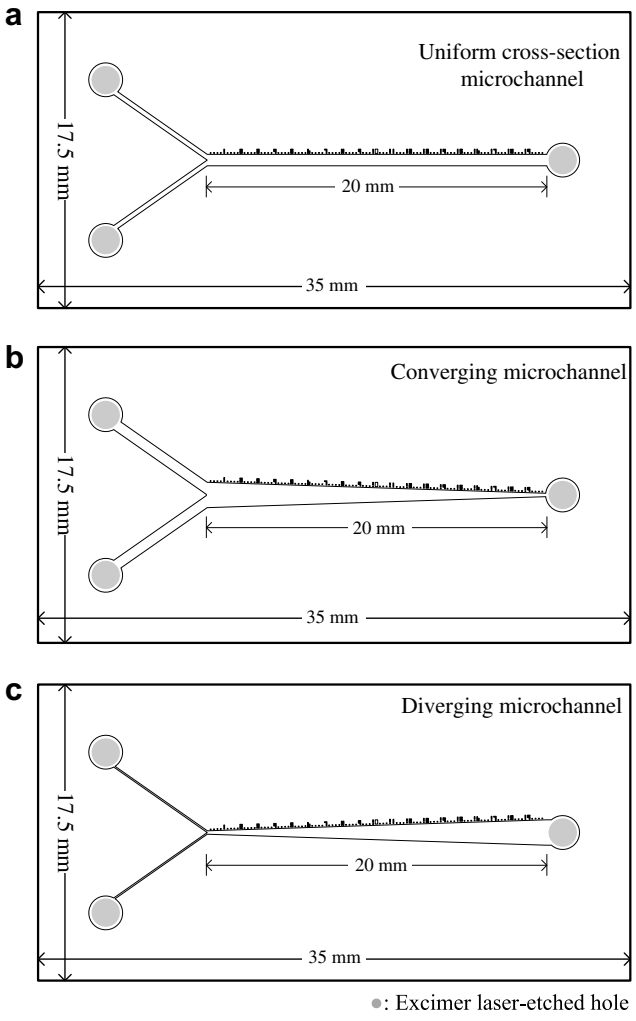

Fig. 2. Schematic of the test sections: (a) uniform cross-section, (b) converging and (c) diverging microchannels.

a uniform cross-section. The dimensions of front and main channels are summarized in Table 1.

2.3. Experimental procedure

This study employed aqueous solutions of sulfuric acid and sodium bicarbonate as the working fluids. Both reactant solutions were driven by the syringe pump at the same flow rate. The volume flow rates (Q) for both solutions were controlled ranging from 0.16×10^{-9} to 2.40×10^{-9} m^3/s, corresponding to the Reynolds number from 0.79 to 12.0 based on mean hydraulic diameter of the main channel and mixture properties; the mass flux, based on the mean cross-section area of the main channel, was controlled ranging from 4.94 to 74.1 kg/m^2 s for the uniform cross-section microchannel and from 3.90 to 58.5 kg/m^2 s for the converging or diverging one. The concentration of both reactants at the inlet was 0.75 mol/L.

2.4. Measurement uncertainty

The measurement uncertainty for the flow rate after calibration using a high precision electronic balance was estimated to be 0.54%. The measurement uncertainty of differential pressure transducer was 1.25 kPa. Moreover, the uncertainty in the measured bubble radii, concentration of sulfuric acid solution, and concentration of sodium bicarbonate solution is 1.08%, 1.89%, and 0.31%, respectively. The experiments were conducted at room temperature of 24 ± 0.5 °C.

3. Theory

3.1. The extended Rayleigh equation

The governing equation for the growth of a spherical bubble in a homogeneous liquid medium, known as the extended Rayleigh equation, is of the form [28]:

$$P_b(t) - P_l - \frac{2\sigma}{R_b} = \rho_l \left[R_b \frac{d^2 R_b}{dt^2} + \frac{3}{2}\left(\frac{dR_b}{dt}\right)^2 \right] + \frac{4\mu_l}{R_b}\frac{dR_b}{dt} \quad (1)$$

where R_b is the instant bubble radius, t is the time, ρ_l is the density of the liquid, σ is the surface tension, μ_l is the viscosity of the liquid, P_b is the pressure in the bubble, and P_l is the pressure in the liquid (a constant, same as the pressure far away from the bubble). The initial condition for Eq. (1) is given as follows:

$$R_b = R_0, \quad \text{at } t = 0 \quad (2)$$

where R_0 is the initial bubble radius.

Note that for a bubble to grow, i.e., $dR_b/dt > 0$, Eq. (1) indicates that the initial bubble radius must be greater than the critical bubble radius ($R_{b,cr}$) by ignoring the inertia and viscous terms [24]:

$$R_0 \geqslant R_{b,cr} = \frac{2\sigma}{P_{b0} - P_l} \quad (3)$$

where P_{b0} is the initial pressure in the bubble.

3.2. Solution for the extended Rayleigh equation under certain conditions

In the initial period, the bubble growth is controlled by liquid inertia. Assuming the pressure in the bubble is constant and neglecting the capillary pressure and viscous force, the bubble would grow with a constant rate as [29]:

$$R_b(t) = R_0 + \left(\frac{2}{3}\frac{P_b - P_l}{\rho_l}\right)^{1/2} t \quad \text{(inertia-force-control)} \quad (4)$$

Table 1
Summary of the dimensions of the test section

Type of the test section	Main channel					Front channel				Inlet and outlet
	Width, in (μm)	Width, out (μm)	Depth (μm)	Length (mm)	D_H (μm)	Width (μm)	Depth (μm)	Length (mm)	D_H (μm)	Radius (mm)
Uniform cross-section	675	675	100	20	174	290	100	6.46	149	1
Converging	1500	210	100	20	174	620	100	6.65	172	1
Diverging	210	1500	100	20	174	100	100	6.22	100	1

On the other hand, if the bubble growth is controlled by viscous force, the bubble would grow exponentially, for $R_{b,cr} \to 0$, as follows [30]:

$$R_b(t) = R_0 \exp\left[\frac{(P_b - P_l)t}{4\mu_l}\right] \quad \text{(viscous-force-control)} \tag{5}$$

Furthermore, when the mass diffusion controls the bubble growth, the bubble radius (with $R_0 = 0$) changes as follows [31,32]:

$$R_b(t) = 2\beta(Dt)^{1/2} \quad \text{(mass-diffusion-control)} \tag{6}$$

where β is the dimensionless growth constant, and D is the diffusion coefficient.

3.3. The bubble growth with chemical reactions

3.3.1. Catalytic bubble model [24]

Favelukis and Yablonsky [24] recently proposed a theoretical model, i.e., catalytic bubble model, for a spherical bubble growing in a stationary liquid with a first-order chemical reaction at the bubble surface. The model further assumes that all gas phase products go into the bubble and no gas product dissolves back to the liquid. The diffusion flux of the reactant (solute) toward the bubble must be equal to the reaction rate per unit area at the bubble surface. Thus

$$\frac{P_{b0}}{R_g T_b}\frac{dR_b}{dt} = D\left(\frac{\partial c}{\partial r}\right)_{r=R_b} = k_s c_s \tag{7}$$

where R_g is the universal gas constant, T_b is the temperature in the bubble, c is the molar concentration of the solute in the liquid, c_s is the molar concentration of the solute at the bubble surface, and k_s is the first-order surface reaction constant, having the unit of length per unit time [33]. The LHS term in the equation assumes that the gas product is an ideal gas and with constant pressure ($P_b = P_{b0}$) and temperature in the bubble.

Favelukis and Yablonsky [24] solved the steady-state diffusion equation for the solute in the liquid assuming the molar concentration of the solute is c_s at the bubble surface and c_∞ far from the bubble. The solute concentration at the bubble surface is expressed as a function of c_∞, k_s, R_b, and D. They then employed Eq. (7) to solve for the instant bubble radius, using the solute concentration at the bubble surface, as follows [24]:

$$R_b(t) = R_0\left\{-\frac{1}{b_0} + \left[\left(1+\frac{1}{b_0}\right)^2 + 2a\tau_0\right]^{1/2}\right\} \tag{8}$$

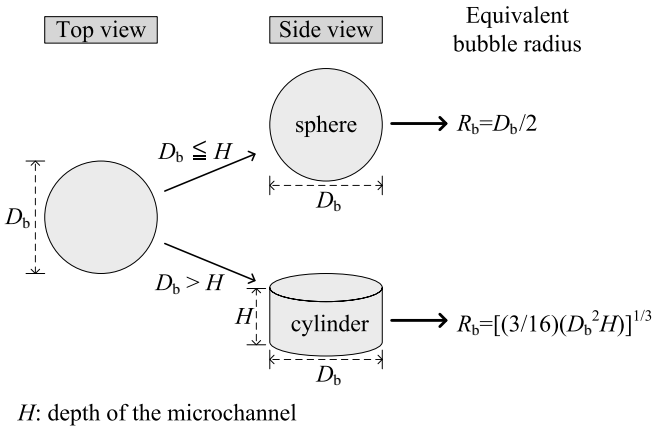

Fig. 3. The equivalent bubble radius (R_b) in the microchannel.

where $a = R_g T_b c_\infty / P_{b0}$ and $b_0 = k_s R_0 / D$ are dimensionless numbers, and $\tau_0 = Dt/R_0^2$ is the dimensionless time. For the case with a fast chemical reaction ($k_s \gg D/R_b$), which can be regarded as a mass-diffusion-control case, Eq. (8) is reduced to:

$$R_b(t) = R_0(1 + 2a\tau_0)^{1/2} \tag{9}$$

Obviously, Eq. (9) is similar to Eq. (6), which the bubble growth is controlled by the diffusion of the gas molecule. Eqs. (6) and (9) indicate that the bubble grows as a square root of the product of the diffusion coefficient and time.

On the other hand, the solution for the case with a slow chemical reaction ($k_s \ll D/R_b$), which is a chemical-reaction-control case, can be written as:

$$R_b(t) = R_0(1 + ab_0\tau_0) \tag{10}$$

Favelukis and Yablonsky [24] also presented numerical results for the bubble growth using the unsteady-state diffusion equation, and the results show that the bubble growth behavior and trend are similar to that of the quasi-steady-state solution from the steady-state diffusion equation. In the present study, the bubble growth for one of the cases was compared with the quasi-steady-state model.

3.3.2. Evaluated from the average mass-transfer coefficient

Favelukis and Yablonsky's catalytic bubble model [24], however, neglected the possibly convective effect on solute transport in the liquid due to relative motion between the bubble and liquid. Considering such a convective effect by employing an average

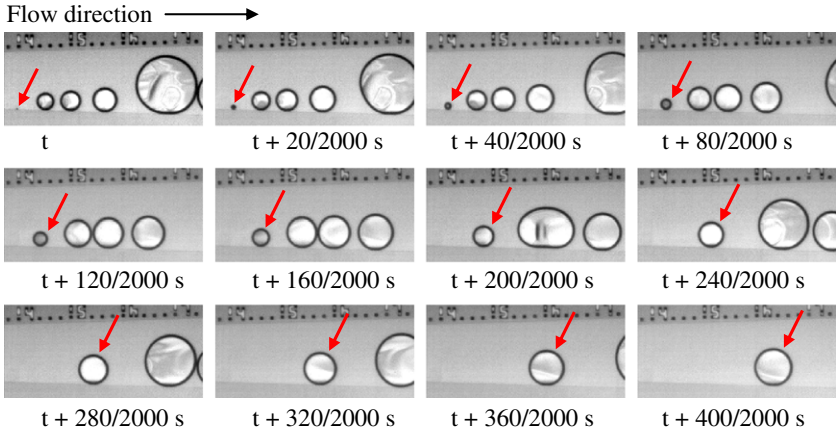

Fig. 4. A series of the images of the bubble growth in the diverging microchannel (case A), $Q = 0.80 \times 10^{-9}$ m^3/s.

mass-transfer coefficient from the bulk liquid to the bubble interface, k_m, the continuity of mass flux at the bubble surface results in:

$$\frac{P_{b0}}{R_g T_b}\frac{dR_b}{dt} = k_m(c_\infty - c_s) = k_s c_s \tag{11}$$

The above equation assumes that the solute transporting to the bubble surface reacts there and the gas product, as an ideal gas, goes into the bubble with constant pressure and temperature in the bubble. The surface concentration can thus be expressed as:

$$c_s = \frac{k_m c_\infty}{k_s + k_m} \tag{12}$$

Substituting Eq. (12) into the RHS of Eq. (11) and after rearrangement gives:

$$\frac{dR_b}{dt} = \frac{a k_s k_m}{k_s + k_m} \tag{13}$$

Assuming the bubble is a sphere, the average mass-transfer coefficient (k_m) may be obtained from the following equation [34]:

$$Sh = 2.0 + 0.6(Re_b)^{1/2}(Sc)^{1/3} \tag{14}$$

where $Sh = k_m(2R_b)/D$ is the Sherwood number, $Re_b = \rho_l u_r(2R_b)/\mu_l$ is the Reynolds number, $Sc = \mu_l/(\rho_l D)$ is the Schmidt number, and u_r is the relative velocity between the sphere and bulk liquid.

For the case with $u_r = 0$, i.e., $Sh = 2.0$, the solution of the bubble radius is the same as Eq. (8) proposed by Favelukis and Yablonsky [24]. On the other hand, for the case with $0.6(Re_b)^{1/2}(Sc)^{1/3} \gg 2.0$, i.e., $Sh \approx 0.6(Re_b)^{1/2}(Sc)^{1/3}$, the average mass-transfer coefficient can be expressed as:

$$k_m = C_1 R_b^{-1/2} \tag{15}$$

where

$$C_1 = \frac{0.6}{2^{1/2}}\left(\frac{\rho_l}{\mu_l}\right)^{1/6} D^{2/3} u_r^{1/2} \tag{16}$$

Substituting Eq. (15) into Eq. (13) yields:

$$\frac{dR_b}{dt} = \frac{a k_s \left(C_1 R_b^{-1/2}\right)}{k_s + \left(C_1 R_b^{-1/2}\right)} \tag{17}$$

The solution of above equation is of the form:

$$\left(R_b^{3/2} - R_0^{3/2}\right) + \frac{3C_1}{2k_s}(R_b - R_0) = \frac{3}{2}C_1 a t \tag{18}$$

For the case with a fast chemical reaction ($k_s \gg C_1 R_b^{-1/2}$), the solution can be simplified as:

$$R_b(t) = \left(R_0^{3/2} + \frac{3}{2}C_1 a t\right)^{2/3} \tag{19}$$

The solution for the case with a slow chemical reaction ($k_s \ll C_1 R_b^{-1/2}$) is the same as Eq. (10).

3.3.3. Constant generation rate of the gas product to the bubble

For a constant generation rate of the gas product to the growing bubble, the change rate of the number of moles of the gas in the bubble can be written as follows:

$$\frac{dn}{dt} = n_g = \text{constant} \quad (\text{mol/s}) \tag{20}$$

where n is the moles of the gas product within the bubble and n_g is the constant generation rate of the gas product into the bubble. Assuming the gas is an ideal one and realizing the pressure difference between the gas and liquid is governed by the Young–Laplace equation:

$$P_b - P_l = \frac{2\sigma}{R_b} \tag{21}$$

Eq. (20) can be re-written as:

$$\left(P_l R_b^2 + \frac{4}{3}\sigma R_b\right)\frac{dR_b}{dt} = \frac{n_g R_g T_b}{4\pi} \tag{22}$$

Integration of the above equation using the initial condition, Eq. (2), gives:

$$\left(R_b^3 - R_0^3\right) + \frac{2\sigma}{P_l}\left(R_b^2 - R_0^2\right) = \frac{3R_g T_b}{4\pi P_l} n_g t \tag{23}$$

For a given time t, the real root for R_b of Eq. (23) can be obtained by the Mathematica as:

$$R_b(t) = \frac{1}{6}\left\{-2C_2 + 2^{4/3}C_2^2[F(t)]^{-1} + 2^{2/3}[F(t)]\right\} \tag{24}$$

where

$$F(t) = \left\{C_3 + 27C_4 t + \left[-4C_2^6 + (C_3 + 27C_4 t)^2\right]^{1/2}\right\}^{1/3} \tag{25}$$

$$C_2 = \frac{2\sigma}{P_l} \tag{26}$$

$$C_3 = -2C_2^3 + 27\left(C_2 R_0^2 + R_0^3\right) \tag{27}$$

$$C_4 = \frac{3R_g T_b}{4\pi P_l} n_g \tag{28}$$

In the present study, $C_2 = (2 \times 73 \times 10^{-3}\ \text{N/m})/(1.013 \times 10^5\ \text{N/m}^2) = 1.44 \times 10^{-6}$ m and $C_3 = 1.79 \times 10^{-14}\ \text{m}^3$. Therefore, the second term in the RHS of Eq. (24) is negligibly small. Moreover, $F(t)$, given by Eq. (25), can be approximated as:

$$F(t) = 2^{1/3}(C_3 + 27C_4 t)^{1/3} \tag{29}$$

and the instant bubble radius can be simplified as follows:

$$R_b(t) = \frac{1}{3}\left[-C_2 + (C_3 + 27C_4 t)^{1/3}\right] \tag{30}$$

$$R_b(t) \approx C_4^{1/3} t^{1/3}, \quad \text{for } t > 0.01 \tag{31}$$

4. Results and discussion

4.1. The equivalent radius determination

In this study, the bubble in the microchannel may be in the form of a sphere ($D_b \leqq H$), or constrained by the top and bottom walls

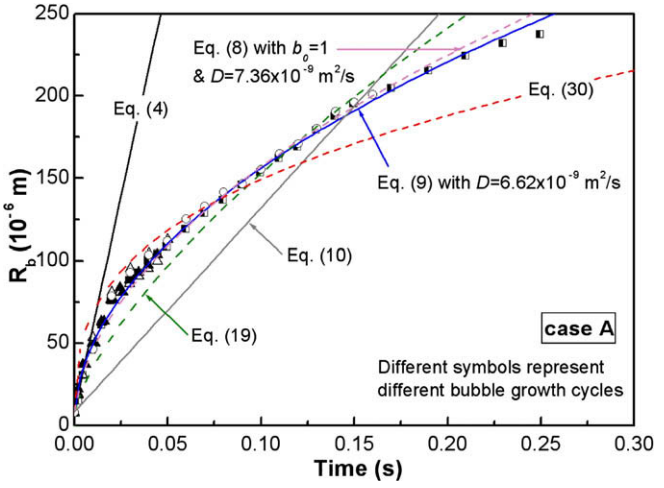

Fig. 5. The time evolution of the equivalent bubble radius in the diverging microchannel (case A), $Q = 0.80 \times 10^{-9}\ \text{m}^3/\text{s}$.

and become a distorted sphere being approximated as a cylinder with height H from the side view ($D_b > H$), as shown in Fig. 3. The bubble growth is analyzed using an equivalent bubble radius (R_b), defined as the radius of a sphere with the same total volume of the bubble measured in the experiments. Thus

$$R_b = \frac{D_b}{2}, \quad \text{for } D_b \leqq H \tag{32}$$

$$R_b = \left(\frac{3}{16} D_b^2 H\right)^{1/3}, \quad \text{for } D_b > H \tag{33}$$

where D_b is the bubble diameter from the top-view image and H is the depth of the microchannel.

4.2. Experimental results of the bubble growth

Experiments were conducted with the volume flow rates ranging from 0.16×10^{-9} to 2.40×10^{-9} m^3/s and inlet concentration for both solutions of sulfuric acid and sodium bicarbonate of 0.75 mol/L. The nucleation and growth of bubbles appeared in the diverging microchannel for $Q = 0.16 \times 10^{-9}$ and $Q = 0.80 \times 10^{-9}$ m^3/s, and the uniform cross-section microchannel for $Q = 0.16 \times 10^{-9}$ m^3/s. No bubble was generated for higher flow rates. The initial bubble radius observed by locally enlarging the site of the bubble nucleation was between 7.41 and 10.6 μm, and the mean initial radius of the bubble was 8.25 μm. As for the converging microchannel, no bubble was nucleated at the given inlet concentration and in the range of flow rate of the present study. This is consistent with what reported by Fu et al. [25]. They found that, in contrast to that in the diverging microchannel, no bubble was formed in the converging microchannel for low inlet concentrations and high volume flow rates. The test section employed by Fu et al. [25], however, included a relatively large inlet chamber, at which both solutions may be mixed with the different degree in different kinds of the microchannels. Such the pre-mixing effect has been eliminated by the proper inlet design, as stated earlier in Section 2 and the bubble nucleation in the microchannel is purely due to the local environment. The following sections present and discuss the results of the bubble growth in four different cases, referred to case A to D in the diverging or uniform cross-section microchannel. The growth characteristics of the selected bubble, a single bubble, were analyzed without any merger occurrence.

4.2.1. Case A: in the diverging microchannel with $Q = 0.80 \times 10^{-9}$ m^3/s

Fig. 4 shows a series of the images of the bubble nucleation and growth in the diverging microchannel with $Q = 0.80 \times 10^{-9}$ m^3/s. The figure illustrates that bubbles are nucleated at the channel wall. The top-view images reveal that the bubble under consideration grows spherically while moving downstream with the liquid flow possibly due to the relatively large flow rate for this case. The ruler etched along the channel enables the determination of the bubble velocity. The mean velocity of the bubble center from the images in Fig. 4, calculated based on the bubble center displacement in a time interval in the figure, is 1.32×10^{-2} m/s. This is very close to the mean velocity of the liquid, 1.33×10^{-2} m/s, at the axial location under consideration. Since the bubble center is from near the wall to about one-third of the channel width from the wall and the mean liquid velocity would be the liquid velocity at this range. It is, therefore, can be assumed that the relatively velocity between the bubble and surrounding liquid is very small and this

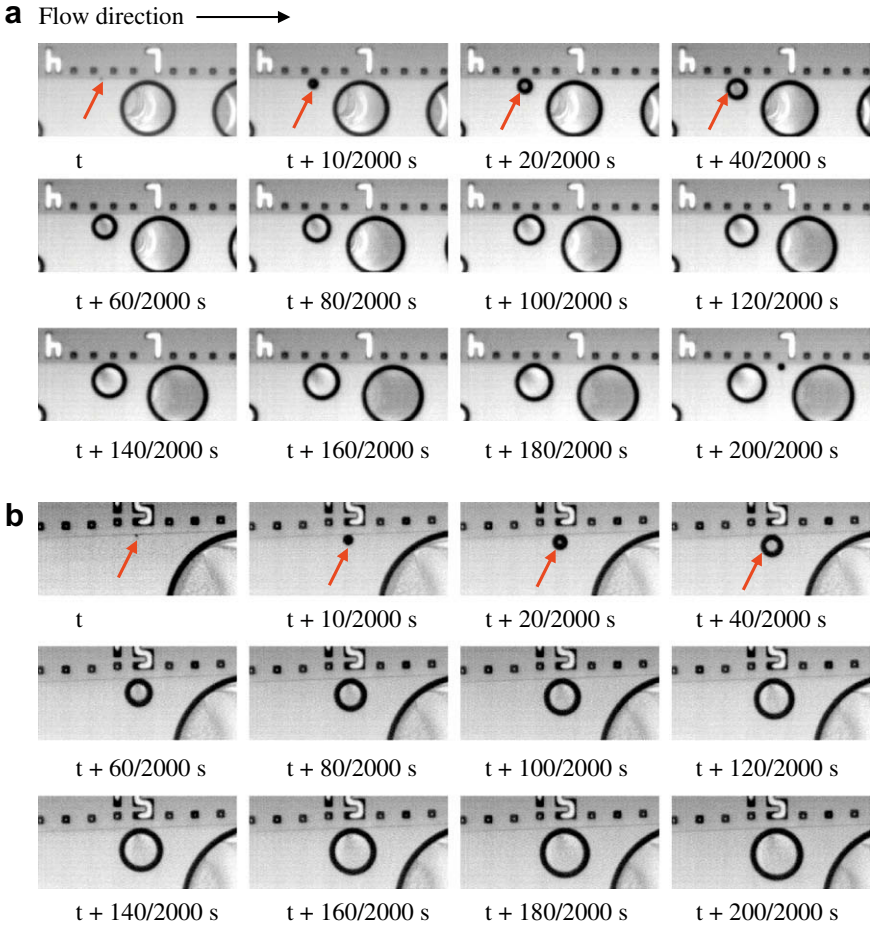

Fig. 6. A series of the images of the bubble growth in the (a) uniform cross-section (case B), and (b) diverging microchannels (case C), $Q = 0.16 \times 10^{-9}$ m^3/s.

case can be treated as the one without relative motion between the bubble and liquid. Moreover, the velocity of the bubble center, estimated from the captured images (Fig. 4), is nearly constant after $t = 0.1$ s. The contact angle of the mixture on the silicon wafer and on the Pyrex #7740 glass has been measured to be about 58° and 19°, respectively. This suggests that both surfaces of silicon wafer and Pyrex #7740 glass are quite hydrophilic. Accordingly, a thin liquid film between the bubble and the channel wall is usually observed. The liquid film may enable the bubble motion in the flow direction once it departs from the wall.

The time evolution of the equivalent bubble radius for case A is shown in Fig. 5. Different symbols in the figure stand for different cycles of the bubble nucleation and growth. It should be noted that the bubble for each cycle may not be nucleated from exactly the same location and good agreements among different cycles are demonstrated. The predictions of the bubble growth from various models presented in the last section are also shown in the figure. For the initial period, i.e., $t < 0.01$ s, the equivalent bubble radius increases linearly, indicating the bubble growth for the beginning period is inertia-force-control. Fig. 5 demonstrates that the equivalent bubble radius grows following a square root of the time and agrees very well with Eq. (9) or Eq. (8) with $b_0 \gg 1$ proposed by Favelukis and Yablonsky [24]. As discussed earlier in the last section, Eq. (9) or Eq. (8) with $b_0 \gg 1$, is for the bubble growth without relative motion between the bubble center and liquid and with a first-order chemical reaction taking place at the bubble surface and all gas product going into the bubble. Moreover, the chemical reaction is fast and the solute diffusion to the bubble surface is the controlling mechanism. The diffusion coefficient estimated from the best fit using Eq. (9) is 6.62×10^{-9} m^2/s, which is reasonable for the diffusion of species in the liquid medium [35]. The first-order surface reaction constant is 8.02×10^{-1} m/s corresponding to $b_0 = 1000$, for which the prediction of Eq. (8) agrees very well with data.

The bubble growth behavior for this particular case shows that the mass diffusion controls the bubble growth with chemical reactions. This result demonstrates the similarity between the diffusion of solute to the bubble surface and the diffusion of heat to the bubble surface for liquid evaporation in the boiling system. Most previously analytical analyses of the bubble growth due to the heat transfer mechanism of boiling or chemical reactions usually take the diffusion effect into account and result in the bubble growing as a square root of the time.

4.2.2. Cases B and C: in the uniform cross-section and diverging microchannels with $Q = 0.16 \times 10^{-9}$ m^3/s

Unlike the bubble growth characteristic for case A, bubbles are nucleated from the channel wall and grow at the nucleation site for cases B and C while the liquid remains flowing in the microchannel. Fig. 6(a) shows a series of the images of the bubble nucleation and growth in the uniform cross-section microchannel with $Q = 0.16 \times 10^{-9}$ m^3/s during the time span of observation. This case is referred to case B. A similar situation for the bubble nucleation and growth in the diverging microchannel with the same flow rate is referred to case C, as shown in Fig. 6(b). For cases B and C, the bubble remains almost at the nucleation site while growing. This is in contrast to case A, in which the bubble moves with the liquid while growing.

Fig. 7(a) and (b) illustrate the time evolution of the equivalent bubble radius for cases B and C, respectively. The comparison between Fig. 7(a) and (b) demonstrates that the bubble nucleation and growth for cases B and C present the similar behavior. In the initial period ($t < 0.01$ s), the bubble radius grows with the time, the same as that for the initial period of case A. The analyses of the bubble growth characteristics show that the bubble radius increases approximately with the 1/3 power of the time. This suggests that the bubble grows with a constant generation rate of the gas product. The best prediction of the bubble growth is Eq. (30) with the constant generation rates (n_g) of 6.41×10^{-9} and 5.27×10^{-9} mol/s for cases B and C, respectively. Since the bubble continually grows at the nucleation site, the bulk liquid flow may supply the reactants continually to the reaction site resulting in a constant generation rate. For case B, Eq. (30) with $n_g = 6.41 \times 10^{-9}$ mol/s tends to show over prediction for $t > 0.08$ s indicating that the gas product generation rate may become smaller after. Although there is relative motion between the bubble and liquid, the comparison between data and model prediction does not support the analysis with strong relative motion between the bubble center and liquid, for which the bubble radius increases with the 2/3 power of the time (see Eq. (19)). This may be explained by the fact that the bubble sticks on the wall while growing. The liquid convection will be present around about half the bubble surface. This will fail the model with convection around the whole bubble.

4.2.3. Case D: in the diverging microchannel with $Q = 0.16 \times 10^{-9}$ m^3/s and bubble-to-bubble interactions

Cases A, B, and C are basically for bubbles growing independently without a significant influence of a neighboring bubble. Bubble-to-bubble interactions are quite often in a boiling system as well as in the present system with bubbles from chemical reactions [25]. For case D, the bubble growth of a small bubble near a big bubble is examined. Fig. 8 illustrates a series of the images of the bubble nucleation and growth at the channel wall and near a

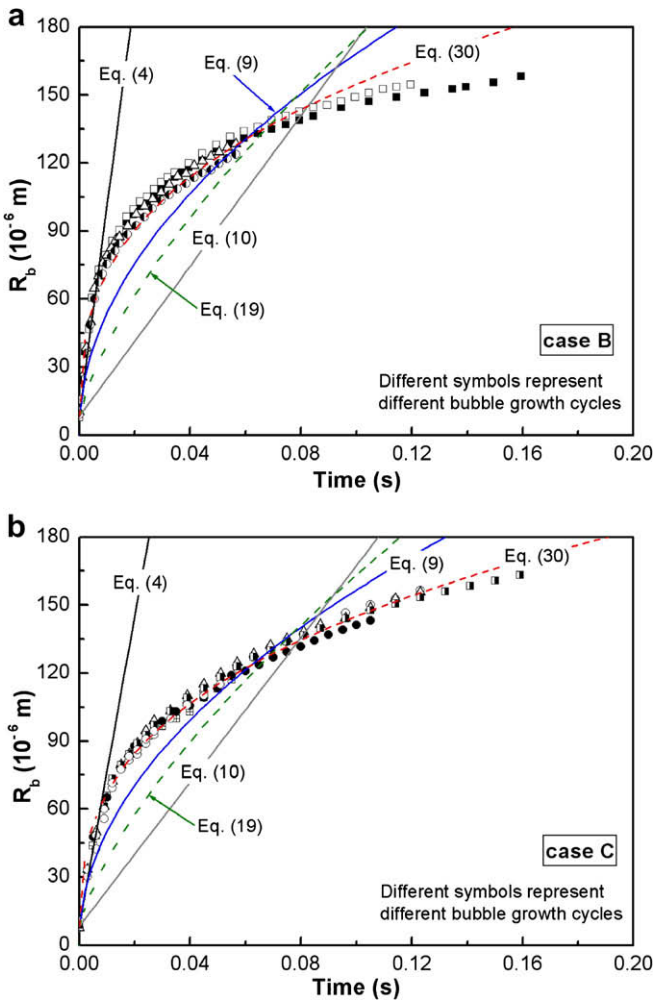

Fig. 7. The time evolution of the equivalent bubble radius in the (a) uniform cross-section (case B), and (b) diverging microchannels (case C), $Q = 0.16 \times 10^{-9}$ m^3/s.

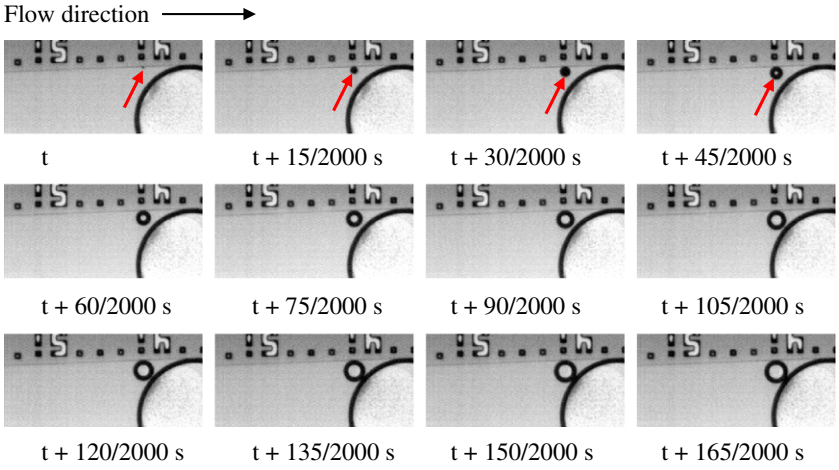

Fig. 8. A series of the images of the bubble growth with bubble-to-bubble interactions in the diverging microchannel (case D), $Q = 0.16 \times 10^{-9}$ m^3/s.

big bubble, in fact, within the shadow of the big one. Bubble-to-bubble interactions between these two bubbles are inevitable. At least, the big bubble would hinder a significant part of the liquid and influence the convection of solute around the bubble under consideration. Eventually, the marked bubble would merge with the big one for this case.

The time evolution of the equivalent bubble radius for case D is presented in Fig. 9. The figure clearly shows that the bubble growth behavior is well predicted by Eq. (30) with a significantly smaller gas generation rate, $n_g = 2.61 \times 10^{-9}$ mol/s, than that for cases B and C. The gas generation rate for case D is approximately a half of that for case C. This significant difference might be caused by the hindering effect of the big bubble. The presence of the big bubble would prevent reactant from entering the down stream side of the bubble under consideration. Consequently, the bubble growth rate is reduced for this case with bubble-to-bubble interactions.

It is interesting to see that bubbles are nucleated at the channel wall for each case of the present study. This result demonstrates that the channel wall material, silicon, might have the catalytic effect for the chemical reaction [36].

Table 2 lists the best fitted equation for all the four cases of this study. Fig. 10 shows that the deviation of the bubble radius between the measurement and predictions is within 10% for case A and 15% for cases B, C, and D.

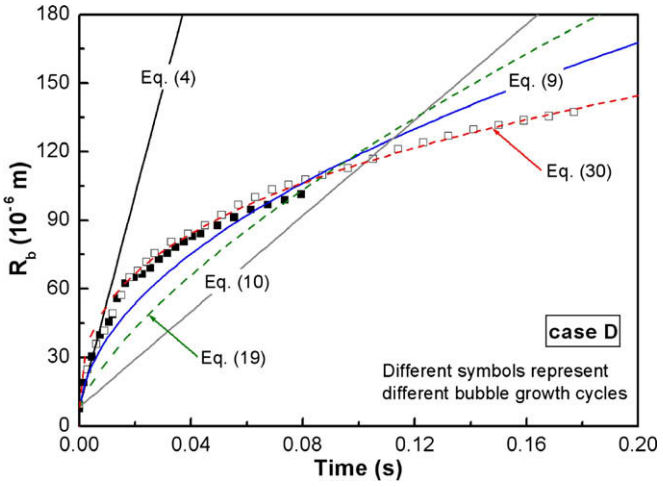

Fig. 9. The time evolution of the equivalent bubble radius with bubble-to-bubble interactions in the diverging microchannel (case D), $Q = 0.16 \times 10^{-9}$ m^3/s.

5. Summary and conclusions

The present work explores the nucleation and growth of CO_2 bubbles due to chemical reactions of sulfuric acid and sodium bicarbonate in three types of microchannels: one with a uniform cross-section, one converging, and another one diverging. The nucleation and growth of bubbles were observed in the diverging microchannel for $Q = 0.16 \times 10^{-9}$ m^3/s (cases C and D) and $Q = 0.80 \times 10^{-9}$ m^3/s (case A), and the uniform cross-section microchannel for $Q = 0.16 \times 10^{-9}$ m^3/s (case B). The theoretical model in the literature has been reviewed and a new model is developed based on the experimental data. The following conclusions may be drawn from the results of the present study:

1. Bubbles are nucleated at the channel wall and the equivalent bubble radius increases linearly during the initial period of the bubble growth, i.e., $t < 0.01$ s, for all the four cases of this study. The initial bubble radius observed is between 7.41 and 10.6 μm, and the mean initial radius of the bubble is 8.25 μm.
2. For case A, with a relatively high flow rate in the diverging microchannel, the bubbles move with the liquid and the bubble growth is found to be controlled by solute diffusion toward the bubble interface. The instant bubble radius can be fitted within ±10% as a square root of the time, proposed by Favelukis and Yablonsky [24].
3. For cases B and C, the bubbles stay almost at the nucleation site while growing and grow with a constant gas product generation rate resulting in the instant bubble radius following the one-third power of the time. The fitted equations agree with experimental data within ±15%.

Table 2
The best fitted equation for each case

Case	The best fitted equation	Corresponding equation
A	$R_b(t) = 8.25 \times 10^{-6}(1 + 3.57 \times 10^3 t)^{1/2}$	Eq. (9)
B	$R_b(t) = \frac{1}{3}[-1.44 \times 10^{-6} + (1.79 \times 10^{-14} + 10.1 \times 10^{-10} t)^{1/3}]$	Eq. (30)
C	$R_b(t) = \frac{1}{3}[-1.44 \times 10^{-6} + (1.79 \times 10^{-14} + 8.31 \times 10^{-10} t)^{1/3}]$	Eq. (30)
D	$R_b(t) = \frac{1}{3}[-1.44 \times 10^{-6} + (1.79 \times 10^{14} + 4.11 \times 10^{-10} t)^{1/3}]$	Eq. (30)

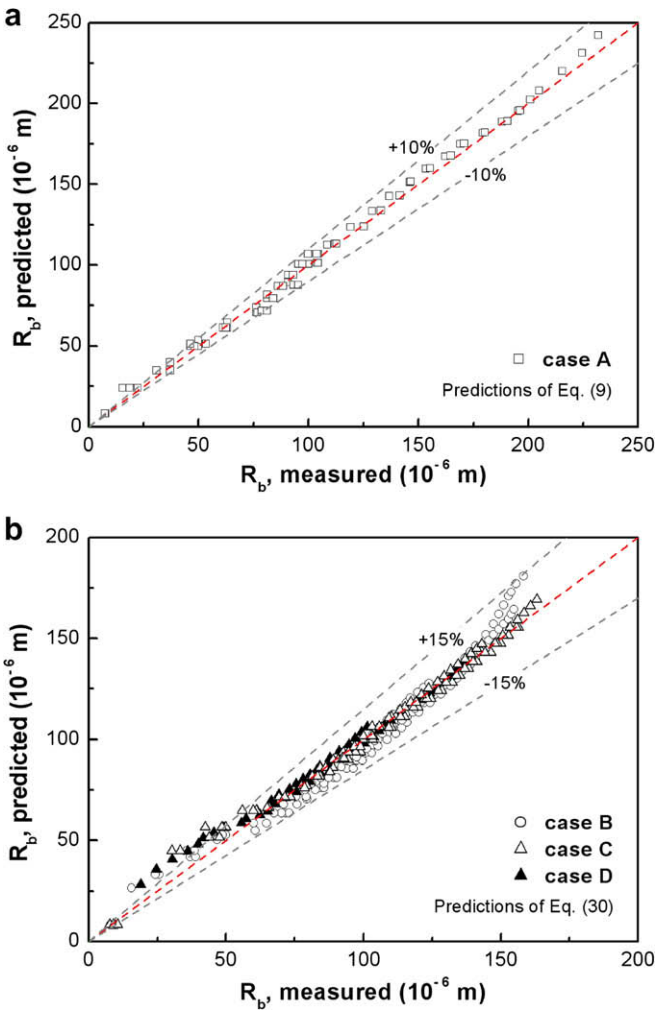

Fig. 10. The comparisons of the equivalent bubble radius between experiments and the best fit of the prediction of the corresponding equation, (a) case A and (b) cases B, C, and D.

4. For case D, the bubble very close to a big bubble also grows with a constant gas product generation rate but a significantly lower generation rate due to the obstructive effect on the liquid convection of the neighboring big bubble.

Acknowledgement

This work was supported by the National Science Council of Taiwan under the contract No. of NSC 95-2218-E-007-112.

References

[1] K. Fei, C.W. Hong, All-angle removal of CO_2 bubbles from the anode microchannels of a micro-fuel cell by lattice-Boltzmann simulation, Microfluidics Nanofluidics 3 (2007) 77–88.
[2] T. Bewer, T. Beckmann, H. Dohle, J. Mergel, D. Stolten, Novel method for investigation of two-phase flow in liquid feed direct methanol fuel cells using an aqueous H_2O_2 solution, J. Power Sources 125 (2004) 1–9.
[3] H. Yang, T.S. Zhao, Q. Ye, In situ visualization study of CO_2 gas bubble behavior in DMFC anode flow fields, J. Power Sources 139 (2005) 79–90.
[4] G.Q. Lu, C.Y. Wang, Electrochemical and flow characterization of a direct methanol fuel cell, J. Power Sources 134 (2004) 33–40.
[5] P. Argyropoulos, K. Scott, W.M. Taama, Gas evolution and power performance in direct methanol fuel cells, J. Appl. Electrochem. 29 (1999) 661–669.
[6] A. Oedegaard, C. Hebling, A. Schmitz, S. Møller-Holst, R. Tunold, Influence of diffusion layer properties on low-temperature DMFC, J. Power Sources 127 (2004) 187–196.
[7] P.C. Lee, F.G. Tseng, C. Pan, Bubble dynamics in microchannels. Part I. Single microchannel, Int. J. Heat Mass Transfer 47 (2004) 5575–5589.
[8] H.Y. Li, F.G. Tseng, C. Pan, Bubble dynamics in microchannels. Part II. Two parallel microchannels, Int. J. Heat Mass Transfer 47 (2004) 5591–5601.
[9] D. Li, V.K. Dhir, Numerical study of single bubble dynamics during flow boiling, J. Heat Transfer Trans. ASME 129 (2007) 864–876.
[10] S.J.D. van Stranlen, The mechanism of nucleate boiling of in pure liquids and in binary mixtures. Part I, Int. J. Heat Mass Transfer 9 (1967) 995–1020.
[11] S.J.D. van Stranlen, M.S. Sohal, R. Cole, W.M. Sluyter, Bubble growth rates in pure and binary systems: combined effect of relaxation and evaporation microlayers, Int. J. Heat Mass Transfer 18 (1975) 453–467.
[12] A.J. Robinson, R.L. Judd, Bubble growth in a uniform and spatially distributed temperature field, Int. J. Heat Mass Transfer 44 (2001) 2699–2710.
[13] B.B. Mikic, W.M. Rohsenow, P. Griffith, On bubble growth rates, Int. J. Heat Mass Transfer 13 (1970) 657–666.
[14] D. Lastochkin, M. Favelukis, Bubble growth in a variable diffusion coefficient liquid, Chem. Eng. J. 69 (1998) 21–25.
[15] M. Favelukis, Z. Zhang, V. Pai, On the growth of a non-ideal gas bubble in a solvent–polymer solution, Polym. Eng. Sci. 40 (2000) 1350–1359.
[16] V. Pai, M. Favelukis, Dynamics of spherical bubble growth, J. Cell. Plast. 38 (2002) 403–419.
[17] N. Divinis, T.D. Karapantsios, M. Kostoglou, C.S. Panoutsos, V. Bontozoglou, A.C. Michels, M.C. Sneep, R. De Bruijn, H. Lotz, Bubbles growing in supersaturated solution at reduced gravity, AIChE J. 50 (2004) 2369–2382.
[18] N. Divinis, M. Kostoglou, T.D. Karapantsios, V. Bontozoglou, Self-similar growth of a gas bubble induced by localized heating: the effect of temperature-dependent transport properties, Chem. Eng. Sci. 60 (2005) 1673–1683.
[19] H.C. Lee, B.D. Oh, S.W. Bae, M.H. Kim, Single bubble growth in saturated pool boiling on a constant wall temperature surface, Int. J. Multiphase Flow 29 (2003) 1857–1874.
[20] H.C. Lee, J. Kim, B.D. Oh, M.H. Kim, Single bubble growth in saturated pool boiling of binary mixtures, Int. J. Multiphase Flow 30 (2004) 697–710.
[21] X. Frank, N. Dietrich, J. Wu, R. Barraud, H.Z. Li, Bubble nucleation and growth in fluids, Chem. Eng. Sci. 62 (2007) 7090–7097.
[22] A. Kapilashrami, A.K. Lahiri, S. Seetharaman, Bubble formation through reaction at liquid–liquid interfaces, Steel Res. Int. 76 (2005) 616–623.
[23] J. Hong, H.S. Woo, Application of the fractional derivatives method to bubble growth/dissolution processes with or without first-order chemical reaction, AIChE J. 31 (1985) 1695–1706.
[24] M. Favelukis, G.S. Yablonsky, Catalytic bubble model: bubble growth with an interfacial chemical reaction, Ind. Eng. Chem. Res. 43 (2004) 4476–4482.
[25] B.R. Fu, F.G. Tseng, C. Pan, Two-phase flow in converging and diverging microchannels with CO_2 bubbles produced by chemical reactions, Int. J. Heat Mass Transfer 50 (2007) 1–14.
[26] Y. Pocker, D.W. Bjorkquist, Stopped-flow studies of carbon dioxide hydration and bicarbonate dehydration in H_2O and D_2O acid–base and metal ion catalysis, J. Am. Chem. Soc. 99 (1977) 6537–6543.
[27] B.R. Fu, C. Pan, Flow pattern transition instability in a microchannel with CO_2 bubbles produced by chemical reactions, Int. J. Heat Mass Transfer 48 (2005) 4397–4409.
[28] S.J.D. van Stralen, R. Cole, Boiling Phenomena, McGraw-Hill, New York, 1979 (Chapter 3).
[29] Van P. Carey, Liquid–Vapor Phase-Change Phenomena, Hemisphere, New York, 1992.
[30] M. Favelukis, R.J. Albalak, Bubble growth in viscous Newtonian and non-Newtonian liquids, Chem. Eng. J. 63 (1996) 149–155.
[31] G. Birkhoff, R.S. Margulies, W.A. Horning, Spherical bubble growth, Phys. Fluids 1 (1958) 201–204.
[32] L.E. Scriven, On the dynamics of phase growth, Chem. Eng. Sci. 10 (1959) 1–13.
[33] E.L. Cussler, Diffusion: Mass Transfer in Fluid Systems, Cambridge University Press, New York, 1984 (Chapter 13).
[34] E.L. Cussler, Diffusion: Mass Transfer in Fluid Systems, Cambridge University Press, New York, 1984 (Chapter 9).
[35] J.N. Murrell, A.D. Jenkins, Properties of Liquids and Solutions, second ed., Wiley, Chichester, 1994 (Chapter 6).
[36] C.T. Yeh, Private Communication, Department of Chemistry, National Tsing Hua University, Hsinchu, Taiwan, 2005.